High manganese concentrations in rocks at Gale crater, Mars

Nina L. Lanza, Woodward W. Fischer, Roger C. Wiens, John Grotzinger, Ann M. Ollila, Agnes Cousin, Ryan B. Anderson, Benton C. Clark, Ralf Gellert, Nicolas Mangold, et al.

AGU PUBLICATIONS

Geophysical Research Letters

RESEARCH LETTER
10.1002/2014GL060329

Key Points:
- ChemCam has observed high manganese concentrations in some Martian rocks
- The abundance of manganese indicates strongly oxidizing conditions
- Some Mars environments were more oxidizing than previously recognized

Supporting Information:
- Readme
- Table S1
- Table S2
- Figure S1

Correspondence to:
N. L. Lanza,
nlanza@lanl.gov

Citation:
Lanza, N. L., et al. (2014), High manganese concentrations in rocks at Gale crater, Mars, *Geophys. Res. Lett.*, *41*, 5755–5763, doi:10.1002/2014GL060329.

Received 29 APR 2014
Accepted 13 JUL 2014
Accepted article online 18 JUL 2014
Published online 25 AUG 2014

High manganese concentrations in rocks at Gale crater, Mars

Nina L. Lanza[1], Woodward W. Fischer[2], Roger C. Wiens[1], John Grotzinger[2], Ann M. Ollila[3,4], Agnes Cousin[1], Ryan B. Anderson[5], Benton C. Clark[6], Ralf Gellert[7], Nicolas Mangold[8], Sylvestre Maurice[9], Stéphane Le Mouélic[8], Marion Nachon[8], Mariek Schmidt[10], Jeffrey Berger[11], Samuel M. Clegg[1], Olivier Forni[9], Craig Hardgrove[12], Noureddine Melikechi[13], Horton E. Newsom[3], and Violaine Sautter[14]

[1]Los Alamos National Laboratory, Los Alamos, New Mexico, USA, [2]Division of Geological and Planetary Sciences, California Institute of Technology, Pasadena, California, USA, [3]Institute of Meteoritics, University of New Mexico, Albuquerque, New Mexico, USA, [4]Now at Chevron Energy Technology Company, Houston, Texas, USA, [5]U.S. Geological Survey, Flagstaff, Arizona, USA, [6]Space Science Institute, Boulder, Colorado, USA, [7]Department of Physics, University of Guelph, Guelph, Ontario, Canada, [8]Laboratoire de Planétologie et Géodynamique, Université Nantes, Nantes, France, [9]Institut de Recherche en Astrophysique et Planétologie, Université Paul Sabatier, Toulouse, France, [10]Department of Earth Sciences, Brock University, Saint Catharines, Ontario, Canada, [11]Department of Earth Sciences, University of Western Ontario, London, Ontario, Canada, [12]School of Earth and Space Exploration, Arizona State University, Tempe, Arizona, USA, [13]Department of Physics and Engineering, Delaware State University, Dover, Delaware, USA, [14]Muséum National d'Histoire Naturelle, Paris, France

Abstract The surface of Mars has long been considered a relatively oxidizing environment, an idea supported by the abundance of ferric iron phases observed there. However, compared to iron, manganese is sensitive only to high redox potential oxidants, and when concentrated in rocks, it provides a more specific redox indicator of aqueous environments. Observations from the ChemCam instrument on the Curiosity rover indicate abundances of manganese in and on some rock targets that are 1–2 orders of magnitude higher than previously observed on Mars, suggesting the presence of an as-yet unidentified manganese-rich phase. These results show that the Martian surface has at some point in time hosted much more highly oxidizing conditions than has previously been recognized.

1. Introduction

Fundamental questions exist about the nature and history of redox processes operating in the Martian surface environments. On Earth, the Great Oxygenation Event ~2.35 Ga marks a major dichotomy in planetary evolution that is tied to the evolution of oxygenic photosynthesis and subsequent rise of atmospheric oxygen [*Cloud*, 1968; *Holland*, 1984]. With surface environments bathed in free molecular oxygen, this transition greatly increased the diversity of redox processes and this is reflected in mineralogy and the distribution of redox-sensitive elements like Fe, Mn, and S in the terrestrial geologic record [*Hazen et al.*, 2008]. The behavior of these elements in the Martian geologic record can provide a powerful context for understanding planetary evolution and unraveling the history of both surface redox conditions and liquid water. It is widely appreciated that the Mars surface is, and perhaps was, "oxidizing" [e.g., *Hunten*, 1979; *Zent and McKay*, 1994; *Christensen et al.*, 2001; *Tosca et al.*, 2005; *McLennan et al.*, 2005; *Goetz et al.*, 2005; *Bibring et al.*, 2006; *Zahnle et al.*, 2008; *Hecht et al.*, 2009; *Leshin et al.*, 2013], but key questions remain: How oxidizing is it? What redox processes have transformed the surface, and when did they occur? Have they changed over time?

To address these questions, it is useful to differentiate the geochemical behavior of iron and sulfur—elements that are readily oxidized by a wide range of oxidants to high-valence states under mildly oxidizing conditions (approximately −100 to 100 mV)—from that of manganese, which is uniquely sensitive to high potential oxidants (≫ 500 mV) [*Stumm and Morgan*, 1996]. On both Earth and Mars, Mn is the third most abundant transition metal in the crust and is present in a wide range of igneous minerals exclusively as Mn(II). Terrestrial basalts have an average abundance of ~0.19 wt % MnO [*Turekian and Wedepohl*, 1961], whereas Martian basalts contain ~0.4 wt % MnO [*Taylor and McLennan*, 2009]. When Mn is chemically weathered from primary igneous minerals (where it substitutes in trace amounts for Fe^{2+}), both significant oxygen fugacities and readily available water are required to drive Mn^{2+} oxidation and cycling. In modern terrestrial environments, Mn cycles among the +II, +III, and +IV oxidation states [e.g., *Post*, 1999; *Tebo et al.*, 2005], but only Mn in high-valence

oxidation states rapidly forms insoluble oxide phases in fluids of circumneutral pH. Thus, Mn is concentrated as oxides only in these highly oxidizing, aqueous environments. Once concentrated, subsequent diagenesis may reduce Mn to the +II state and stabilize it as concentrations of Mn(II)-rich minerals, but such phases still reflect the past presence of both water and a strongly oxidizing environment. This is the redox chemistry that concentrates Mn in sedimentary rocks on Earth (including carbonates and sulfates) [*Maynard*, 2010].

Despite a lack of O_2, for over 2 Ga the early anaerobic Earth was characterized by rich redox cycles of Fe and S, but not Mn [*Raiswell and Canfield*, 2012; *Bontognali et al*., 2013; *Halevy*, 2013; *Fischer and Knoll*, 2009]. Indeed, with a notable exception [see *Johnson et al*., 2013], concentrated Mn deposits do not occur until after the flux of O_2 to Earth surface environments provided by oxygenic photosynthesis. On Mars, Mn has been observed as a trace constituent of igneous minerals [e.g., *McSween et al*., 2004; *Yen et al*., 2007; *Schmidt et al*., 2014], but has not been observed in concentrated amounts. Both orbital and rover observations of the chemistry and mineralogy of "modern" soils [*Taylor and McLennan*, 2009; *Meslin et al*., 2013], dust [*Morris et al*., 2006], coatings and weathering rinds [*Herkenhoff et al*., 2004; *Morris et al*., 2004; *Haskin et al*., 2005], and ancient sedimentary rocks [*Tosca et al*., 2005; *McLennan et al*., 2005; *Hurowitz et al*., 2010] show that redox processes operating in the Martian surface environments were capable of oxidizing iron (to ferric oxides, salts, and clays) and sulfur (to sulfate salts), but no evidence for processes that could have oxidized Mn has been observed up to now. Here we describe a wide range of Mn-rich materials that have been observed in rock targets in the first 360 Martian days (sols) of the Curiosity rover's traverse in Gale crater. These materials contain Mn abundances that are 1–2 orders of magnitude higher than previously observed on Mars.

2. Measuring Manganese Abundance With ChemCam

Manganese can be detected by the ChemCam instrument suite on board the Curiosity Mars rover. ChemCam consists of a laser-induced breakdown spectroscopy (LIBS) instrument and a remote micro-imager (RMI). The LIBS provides information about the chemical composition of a target remotely at a microbeam scale (350–550 μm diameter) while the RMI provides high-resolution (40 μrad) images of the geological context for LIBS analysis locations [*Wiens et al*., 2012; *Maurice et al*., 2012]. Although Mn emission peaks are found throughout the ultraviolet and visible LIBS spectral ranges (Figures 1a–1c), many of these peaks overlap with peaks from other elements (notably Fe). However, the spectral region 403–404 nm Mn peak emission lines have essentially no interferences from other elements (Figure 1c) [*Cousin et al*., 2011]. This offers an advantageous diagnostic region for observing Mn in ChemCam data.

To assess the abundance and distribution of Mn detections in rock targets over the rover's traverse in the first 360 sols, the area under the Mn doublet at 403.19 and 403.42 was quantified using LIBS spectra at each target sampling location. The LIBS spectra were first processed to remove the electron continuum (bremsstrahlung) and the nonlaser-induced background, to denoise the spectrum, and to calibrate for wavelength and instrument response [see *Wiens et al*., 2013]. In order to account for small fluctuations in the laser intensity due to variations in laser power or changes in sample coupling, the data are then normalized so that individual shot intensities may be directly compared [*Wiens et al*., 2013; *Clegg et al*., 2009]. Here LIBS data are normalized by spectrometer range (UV, VIO, and VNIR) by dividing each channel by the sum of the total intensity in each range such that the sum of all channels in a given range is equal to 1.

Peak areas were calculated for the shot-averaged spectrum of all but the first five shots at each location; the removal of the first five shots in the shot-averaged spectra is to avoid including a surface dust composition in the spectral data of the rocks. Peak areas were also calculated for each single-shot spectrum, with each analysis consisting of 30 laser shots per location with some exceptions.

In order to quantify the Mn peak areas observed in ChemCam data, 10 standards containing Mn abundances between 0.43 and 76 wt % MnO were analyzed in the laboratory with the ChemCam engineering model under a Mars-like atmosphere of 7 torr CO_2. Two standards have < 0.60 wt % and the remaining eight have Mn abundances > 18 wt % MnO (Table S1 in the supporting information). Standards were prepared as pressed powered (<60 μm) pellets and analyzed at an equivalent power density to the Mars observations. Each standard was analyzed with 50 laser shots (obtaining 50 spectra) per location in three locations, which were averaged to provide a bulk composition. Spectra were processed in the same way as ChemCam data, as described above.

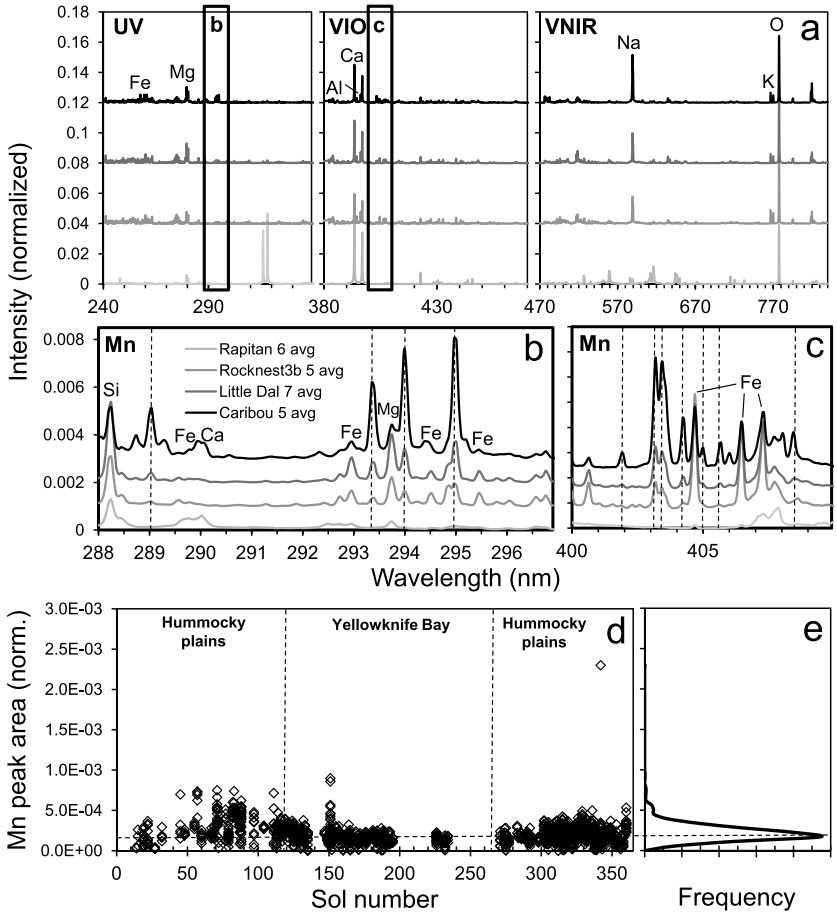

Figure 1. Manganese peaks in the Martian LIBS spectra and the distribution of Mn peak areas in all Martian rocks analyzed in the first 360 sols. Note that the legend shown in Figure 1b also applies to the data shown in Figures 1a and 1c. (a) The shot-averaged spectra for Rapitan (sol 135), Rocknest-3b (sol 82), Little Dal (sol 151), and Caribou (sol 342) in the ultraviolet (UV), violet (VIO), and visible and near-infrared (VNIR) spectral ranges. Rapitan consists predominantly of calcium sulfate and has some of the lowest Mn detections in the first 360 sols, while Caribou contains the highest observed Mn abundance on Mars to date. (b, c) Close-up view of important Mn peaks in the UV and VIO spectral ranges. The triple peak in Figure 1c was used to determine peak areas and Mn abundance in all rocks in the first 360 sols, shown in Figure 1d. (e) The distribution of Mn abundance in rock samples indicates that most observations are low but there are a number of locations containing unusually high Mn.

Peak areas from the 10 Mn standards were used to build a least squares regression model after the methods of *Ollila et al*. [2014]. Individual shot spectra from laboratory standards were used rather than averages. Root-mean-squared error of prediction (RMSEP) is used here for the modeling error assessment. The limit of detection for Mn in LIBS is ~0.06 wt % MnO based on the abundance below which it is difficult to model peak areas correctly.

In addition to the targets analyzed on Mars and the terrestrial standards analyzed in the lab, a terrestrial rock varnish sample N6B was measured in the laboratory to provide a measure of model performance. The N6B Mn abundance was quantified via energy dispersive spectroscopy (EDS) and was found to be ~25–30 wt % MnO throughout the varnish [*Lanza et al*., 2012]; although rock varnish is dominantly composed of MnO_2, the Mn abundances here are represented as MnO for ease of comparison.

Wherever possible, Mn abundances from ChemCam are compared to Alpha Particle X-ray Spectrometer (APXS) data on the same or nearby targets. Although both instruments measure element abundances, ChemCam and APXS measurements differ in two important ways. First, the APXS field of view (1.7 cm diameter in contact) is substantially larger than a ChemCam analysis spot (350–500 μm depending on target distance). Because of this, APXS is less sensitive to trace mineral grains than is ChemCam. Unless the high Mn material is broadly

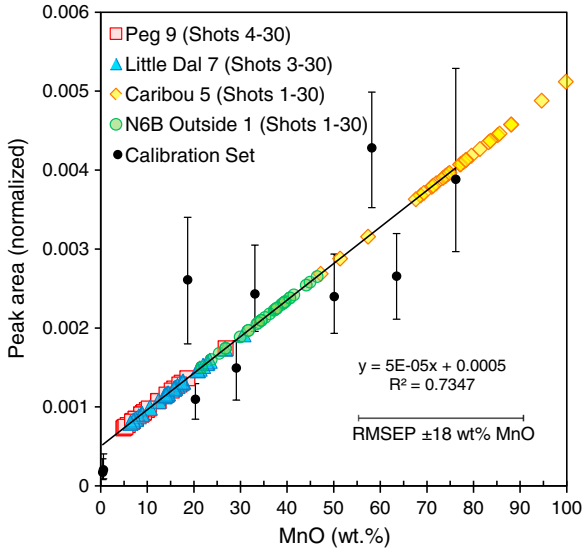

Figure 2. Univariate model of Mn abundance in the Martian samples Caribou (sol 342, yellow diamonds), Little Dal (sol 151, blue triangles), and Peg (sol 71, red squares) with a laboratory sample N6B (green circles) of terrestrial rock varnish for comparison. Here the single-shot calibration set data (10 standards) is represented with averages (black circles) and the minimum and maximum Mn peak areas for each standard (range bars), although single-shot data were used in the model. Note that the predicted Mn abundance for many Caribou locations is above that of the highest calibration standard (~76 wt % MnO). Initial Martian shots containing dust were not modeled, as indicated in the legend. The RMSEP for modeled compositions is ±18 wt % MnO.

distributed within the APXS field of view, it may not be readily observed by APXS as an enrichment. In contrast, the ChemCam sampling footprint is small enough to sample individual mineral phases within a rock. Second, in contrast to ChemCam's ablation sampling method in which each subsequent shot samples at a greater depth, the information depth of APXS is relatively static and dependent on the element being analyzed (~70 μm for Mn in a basaltic matrix [*Campbell et al.*, 2009]). Thus, ChemCam samples a small number of mineral grains or even single grains occupying a small volume in each sampling location [*Maurice et al.*, 2012; *Sautter et al.*, 2014], and APXS is more likely to integrate Mn X-ray counts over a greater number of mineral grains in a larger sample volume [*Gellert et al.*, 2006; *Schmidt et al.*, 2014]. As a result, ChemCam provides a finer-scale observation of the distribution of Mn in individual targets. If Mn is concentrated in a coating or layer rather than discrete mineral grains, the continuity of such coatings can also affect the amount of Mn that APXS detects. It is important to note that ChemCam has also obtained many more analyses (2156 analysis locations) in the first 360 sols than did APXS (66 locations), making it more likely that ChemCam will encounter a relatively rare phase.

3. Manganese Abundance Results

Results for manganese abundance in Mars targets in the first 360 sols are shown as shot-averaged Mn peak areas by sampling location (Figures 1d and 1e). The distribution of Mn peak areas is skewed, with a heavy tail indicating a subpopulation of analyses with high Mn abundances (Figure 1e). Sixty sampling locations are two standard deviations from the mean, containing Mn peak areas significantly higher than the majority of rocks (1750 rock sampling locations) analyzed in the first 360 sols and corresponding to Mn abundances $>$ 1.3 wt % MnO (Table S2 in the supporting information). This discretionary limit represents Mn concentrations that are at least 3 times the mean in the Martian basalts (~0.4 wt % MnO); observations that are 2 orders of magnitude greater than the Martian mean are also included in the $>$ 2 sigma range.

The abundance calibration curve is shown in Figure 2 along with the results for Mars targets containing the highest Mn abundances and the terrestrial rock varnish N6B. The maximum Mn abundance in N6B was modeled as ~45 wt % MnO in N6B location 1 with an RMSEP of ±18 wt % MnO; this range encompasses the measured EDS values (~28 wt % MnO). It should be noted that the EDS measurements were not made at the exact same locations as the LIBS analyses, so the "true" Mn values represented by the LIBS data may be somewhat different than the EDS values. The highest Mn peak area observed on Mars in the first 360 sols (e.g., for Caribou location 5) exceeded that of the most Mn-rich standard (IGS29; Table S1 in the supporting information) that contains 76 wt % MnO. Most samples, both Martian and terrestrial, are well described by the model except for a few Martian shots that contain significant dust, which is low in Mn [e.g., *Meslin et al.*, 2013] and not modeled here.

Occurrences of Mn-enriched rocks are distributed across the rover's traverse (Figure 3a). These 60 sampling locations are from 15 rocks primarily located in two regions: Rocknest (Glenelg formation) and Yellowknife

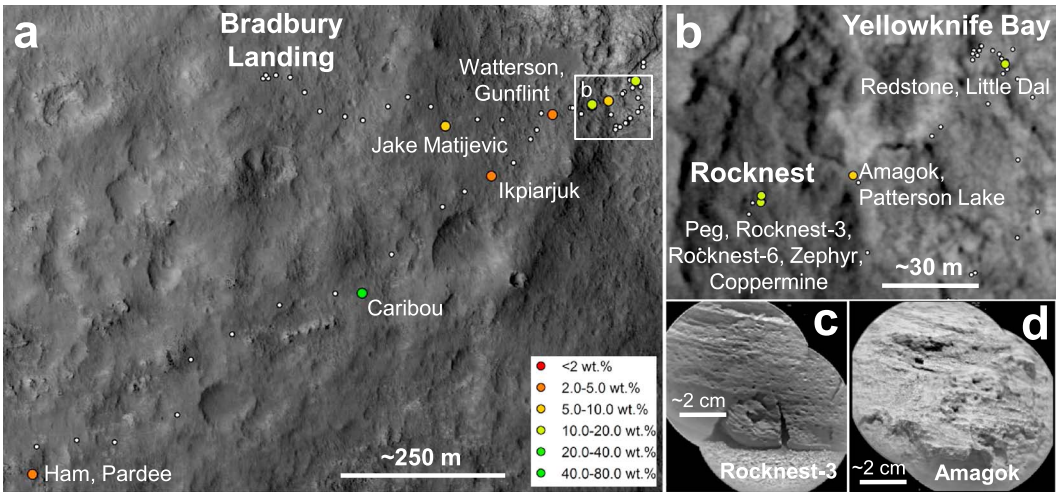

Figure 3. (a) Traverse map showing 60 locations of elevated Mn abundance in the first 360 sols of the mission. White circles represent rover stops along the traverse, while colored circles represent sampling locations; relative Mn abundance is indicated by color from lower (red) to higher (green). (b) Both the Yellowknife Bay and Rocknest regions have multiple high Mn locations on individual rocks. (c) Nearly all rocks containing elevated Mn are fine-grained and dark-toned (Rocknest-3, sol 57, shown) except for (d) two light-toned rocks that are located close to one another: Coppermine (sol 97) and Amagok (sol 111, shown).

Bay (Sheepbed/Gillespie Lake formations) (Figure 3 and Table S2 in the supporting information). When not directly part of outcrops, high Mn rocks are closely associated with nearby outcrops, except for six apparent float rocks: Jake Matijevic (sol 45), Patterson Lake (sol 114), Watterson (sol 329), Gunflint (sol 329), Ikpiarjuk (sol 336), and Pardee (sol 360). The highest observed Mn is in a target named Caribou (sol 342), located at a distance from the other samples in Bradbury rise in the hummocky unit to the southwest of Yellowknife Bay (Figure 3a). It has a normalized Mn peak area that is approximately twice that of the next highest value (Figure 1d) and a Mn abundance of $>$ 60 wt % MnO.

The Rocknest outcrop is located in the middle part of the Glenelg formation, which occurs stratigraphically above the Gillespie Lake and Sheepbed members [*Grotzinger et al.*, 2014]. Rocknest rocks appear generally wind scoured and abraded [*Bridges et al.*, 2013] and have basaltic compositions with fine-grained, sedimentary textures [*Grotzinger et al.*, 2014]. Local soils also have a basaltic composition [*Blake et al.*, 2013; *Bish et al.*, 2013]. Measurements with both ChemCam and APXS show that Rocknest targets are unusually high in Fe and depleted in Mg [*Schmidt et al.*, 2014]. Four rocks in this region were found to have elevated Mn values in at least some ChemCam spectra, including Rocknest-3 (sols 57, 77, 82, 83, and 88), Peg (sol 71), Rocknest-6 (sol 71), and Zephyr (sol 71). All four Rocknest rocks are similar in texture and composition [*Schmidt et al.*, 2014]. Rocknest-3 in particular was extremely well sampled by ChemCam, having been targeted with five sequences for a total of 1950 individual laser shots (spectra) obtained on the side and top of the rock. Out of 46 discrete sampling locations, 31 contained Mn abundances greater than 2 sigma above the mean; this represents 1200 spectra or ~61% of all ChemCam data obtained on this target. The Rocknest-3 ChemCam data had Mn abundances up to 10 wt % MnO (Table S2 in the supporting information), while the single APXS measurement of the top of Rocknest-3 (on the rock edge in a place not targeted by ChemCam) found 0.45 wt % MnO [*Schmidt et al.*, 2014].

The Yellowknife Bay area contains two rocks with elevated Mn in ChemCam data: Redstone (sol 151) and Little Dal (sol 151). These targets contain the second and third largest Mn peak areas, respectively, of all rocks sampled along the traverse. Both rocks were part of a larger structure known as the "Snake," interpreted to be an intrusive sedimentary dike that cuts across the sandstones and mudstones of the Sheepbed and Gillespie Lake formations and is similar in composition and texture to the host rocks [*Grotzinger et al.*, 2014; *McLennan et al.*, 2014]. ChemCam measurements showed one location on Redstone containing 11.8 wt % MnO, while Little Dal contained 1.5–4 wt % MnO in five sampling locations. Although APXS did not sample either Redstone or Little Dal, it did analyze another target on the Snake called Snake River (sol 147) and observed 0.35 wt % MnO [*McLennan et al.*, 2014], consistent with ChemCam measurements on the same target showing less abundant Mn as compared to the other two Snake targets.

In many samples, the ChemCam individual-shot data show distinct Mn peak intensity trends by shot number (depth) (Figure S1 in the supporting information), revealing that Mn is tied to spatially discrete phases in rock targets. Trends in Mn are variable and may be increasing or decreasing with depth depending on location. Several locations on rocks including Caribou, Rocknest-3, and Little Dal show decreasing trends with depth that are consistent with a Mn-rich layer [*Lanza et al*., 2013, 2014a, 2014b], but other locations show invariant (e.g., Redstone) or increasing (e.g., Amagok) trends with shot number that suggest Mn concentration within these fine-grained sedimentary rocks is complex and not limited to surface weathering. For rocks that show at least one high Mn location, other sampling locations on the same rock do not always show a high Mn signal; both Caribou and Jake Matijevic (sol 45) only show one distinctly high Mn location out of several sampled. This is consistent with laboratory measurements of terrestrial rock varnish, which show significant variability in Mn abundance depending on sampling location [*Lanza et al*., 2014b].

Rocks containing high Mn concentrations >1.3 wt % MnO are generally dark, fine-grained, and relatively smooth (Figure 3c), although two targets near to one another (Coppermine, sol 97; and Amagok, sol 111) are brighter and have a more faceted texture (Figure 3d). No individual grains were resolvable in RMI images (Figure 3c and 3d), suggesting a typical grain size < 100 μm, which is also smaller than the LIBS laser analysis spot size of 350–500 μm in diameter. As a result, the spatially discrete high Mn abundances, both between analysis locations on a given rock and within a given sampling location, suggest that the high Mn detections are likely not due to the laser sampling single large, high Mn grains. In particular, the well-sampled Rocknest-3 target contains elevated Mn in a majority of sampling locations, suggesting the presence of a broadly distributed, fine-grained Mn phase. There are no compositional trends apparent in high Mn rocks; observations containing high Mn typically show the elemental profile of the bulk rock, which is attenuated when Mn abundances are high.

4. Discussion

The presence of such high Mn concentrations in and on a spatially wide range of rocks at Gale crater indicates the precipitation of Mn mineral phases, which is only possible in a highly oxidizing, aqueous environment capable of producing sufficient concentrations of high potential oxidants to drive Mn oxidation. Thus far, the identity of the Mn-bearing materials remains unknown. The prevalence of dark-toned Mn-rich targets is consistent with a range of Mn oxide phases like birnessite for at least some targets. Current observations cannot uniquely determine whether the Mn-rich materials comprise sedimentary grains produced elsewhere (e.g., the upslope alluvial fan or the Gale crater rim) and transported to the site of deposition by fluvial sediment transport processes [*Grotzinger et al*., 2014] or whether they are authigenic phases precipitated in situ. Indeed, both processes may have acted, as the observed Mn enrichments cannot be limited solely to modern weathering of ancient rocks due to the low amount of apparent alteration observed [*McLennan et al*., 2014]. Both cosmogenic isotope ratio data [*Farley et al*., 2014] and the presence of the Snake sedimentary dike [*Grotzinger et al*., 2014] suggest that sedimentation rates were high; if the Mn-rich phases were produced within the catchment or as early authigenic grains and cements, the Mn oxidation rates must have been rapid. Alternatively, Mn phases may have been deposited by later diagenetic fluids, which are inferred from the existence of features such as sulfate veins [*Nachon et al*., 2014]. Preexisting Mn phases may also have been remobilized during these diagenetic events to produce features such as coatings on rock surfaces. However, only a subset of Mn detections shows depth trends consistent with a coating or layer; many others show Mn enrichments that are likely integrated phases (e.g., grains) within sedimentary rocks. Overall, the localized nature of the Mn enrichments suggests that conditions leading to efficient Mn oxidation were not always present, and several types and generations of Mn-bearing materials may be present.

Knowledge of the mineralogy of the high Mn materials provides information about the oxidation state of Mn within these phases, which gives important clues about the environments in which they formed. In the terrestrial geologic record of Mn-rich rocks, sediments that were originally enriched in Mn due to the concentration of Mn(IV) oxides now contain mixed-valence oxides and Mn(II) carbonates due to reduction during diagenesis [*Maynard*, 2010; *Johnson et al*., 2013]. A wide range of redox titrants, including ferrous iron and a range of reduced organic carbon and sulfur compounds, can also readily reduce Mn oxides. Reduction to low- and mixed-valence materials could also have occurred for some or all of the materials observed in the Bradbury Rise and Yellowknife Bay regions. Additionally, Mn oxides would themselves have comprised a critical pool of strong oxidants in the environments captured by the rock record of this region. Manganese oxides can be a major vector for the anaerobic oxidation of organic matter [*Sunda and Kieber*, 1994]. In this

regard, determining the material and redox state of Mn preserved in these diagenetically stabilized rocks is important because it will inform the potential taphonomy of organic biosignatures. If these Mn phases remain oxides, it is less likely that their host rocks will preserve organic carbon where it once present. Despite this, the presence of Mn-rich materials provides an additional indicator of a habitable environment because of the variety of habitable aqueous environments in which they form, including hydrothermal systems, oceans, and lakes [*Crerar et al*., 1980].

Because the existence of Mn-rich materials indicates the presence of strongly oxidizing, aqueous environments on or near the Martian surface, this raises the question of what the participating oxidants might have been. There are several possible thermodynamically favorable oxidants, all of which involve high-valence oxygen-bearing species (like O_2) or compounds created by high-valence oxygen-bearing species (like perchlorate). However, Mn(II) oxidation by many of these oxidants is strongly kinetically limited [*Morgan*, 2005; *Luther*, 2010] and sluggish even under the O_2 concentrations on modern Earth (half-life of 400 days for homogeneous oxidation by O_2 at 0.21 atm, or 4 orders slower than Fe oxidation [*Morgan*, 2005]). Oxidation on Mars in the absence of water is hypothesized to occur via photooxidation [*Zent and McKay*, 1994; *Hurowitz et al*., 2010], but for Mn this process is 3 orders of magnitude slower than for Fe and inefficient in solutions that contain dissolved Fe [*Anbar and Holland*, 1992]. Perchlorate is another strong oxidant present on Mars, but it is remarkably stable in water and has a large kinetic barrier to reaction due to its poor nucleophilic and coordinating ability, and thus provides a poor oxidant for Mn [*Sellers et al*., 2007]. Superoxide is produced on Mars by single-electron reduction of O_2 and could have provided useful terminal oxidants for Mn^{2+}(aq) [*Yen et al*., 2000], although Mn(II) can act as a catalytic scavenger for both superoxide and H_2O_2 and inhibit the production of Mn oxides from these species [*Archibald and Fridovich*, 1982; *Horsburgh et al*., 2002]. On Earth, superoxide is used by diverse groups of microbes to catalyze Mn oxidation by reducing O_2 to superoxide and reacting this superoxide with Mn(II) [e.g., *Learman et al*., 2013; *Hansel et al*., 2012], though it is not clear that they conserve energy by doing so [*Tebo et al*., 2005]. However, even with biological catalysis, Mn oxidation rates are exceedingly slow (approximately 0.1 g L^{-1} kyr^{-1}) [*Johnson et al*., 2013], particularly at the low O_2 concentrations (mixing ratio of 1.45×10^{-3}) observed in the present-day Mars atmosphere [*Mahaffy et al*., 2013], although biological catalysis can allow Mn oxidation to proceed even at extremely low (submicromolar) oxygen concentrations [*Clement et al*., 2009]. If the Martian atmospheric O_2 concentrations were higher in the past, perhaps when the atmosphere was thicker, the development of Mn enrichments in the Yellowknife Bay formation and associated rocks of Bradbury Rise is more easily understood.

The Mn enrichments observed in rocks of the Yellowknife Bay formation and Bradbury Rise reveal that the surface of Mars has hosted a history of redox chemistry richer than previously recognized. We observe that certain Mars surface environments must have been capable of producing Mn oxides during or after the aqueous dissolution of primary igneous minerals. Manganese oxides play an important role in environmental chemistry as powerful oxidants and strong sorbents, and can provide highly favorable substrates for microbial respiration [*Myers and Nealson*, 1988]. Thus, although the oxidizing conditions that high Mn materials indicate would not be favorable to organic preservation, the presence of Mn oxides supports the interpretation of a once-habitable aquatic environment on Mars in Gale crater [*Grotzinger et al*., 2014]. Finally, the Martian surface chemistry capable of Mn oxidation marks an era that did not occur on Earth until after the evolution of oxygenic photosynthesis. This result draws a key distinction between Earth and Mars and suggests markedly different modes of planetary redox evolution.

Acknowledgments

The data reported here are archived at the Planetary Data System, available at http://pds-geosciences.wustl.edu/missions/msl/index.htm. This research was carried out with funding from NASA's Mars Program Office and the Centre National d'Etudes Spatiales (CNES) in France. We are grateful to Bradley Tebo and an anonymous reviewer for providing valuable feedback.

The Editor thanks Bradley Tebo and an anonymous reviewer for their assistance in evaluating this paper.

References

Anbar, A. D., and H. D. Holland (1992), The photochemistry of manganese and the origin of banded iron formations, *Geochim. Cosmochim. Acta*, *56*, 2595–2603.

Archibald, F. S., and I. Fridovich (1982), The scavenging of superoxide radical by manganous complexes: In Vitro, *Arch. Biochem. Biophys.*, *214*(2), 452–463.

Bibring, J.-P., et al. (2006), Global mineralogical and aqueous Mars history derived from OMEGA/Mars Express data, *Science*, *312*, 400–404.

Bish, D. L., et al. (2013), X-ray diffraction results from Mars Science Laboratory: Mineralogy of Rocknest at Gale crater, *Science*, *341*, doi:10.1126/science.1238932.

Blake, D. F., et al. (2013), Curiosity at Gale crater, Mars: Characterization and analysis of the Rocknest sand shadow, *Science*, *341*, doi:10.1126/science.1239505.

Bontognali, T. R. R., W. W. Fischer, and K. B. Föllmi (2013), Siliciclastic associated banded iron formation from the 3.2 Ga Moodies group, Barberton greenstone belt, South Africa, *Precambrian Res.*, *226*, 116–124.

Bridges, N. T., S. Le Mouélic, Y. Langevin, K. E. Herkenhoff, S. Maurice, P. Pinet, R. C. Wiens, M. A. de Pablo, N. O. Renno, and the MSL Science Team (2013), Rock abrasion textures seen by the ChemCam Remote Micro-Imager, MSL 44th Lunar and Planetary Science Conference, 18–22 Mar., Houston, Tex., no. 1214.

Campbell, J. L., M. Lee, B. Jones, S. M. Andrushenko, N. G. Holmes, J. A. Maxwell, and S. M. Taylor (2009), A fundamental parameters approach to calibration of the Mars Exploration Rover Alpha Particle X-ray Spectrometer, *J. Geophys. Res.*, *114*, E04006, doi:10.1029/2008J3003272.

Christensen, P. R., R. V. Morris, M. D. Lane, J. L. Bandfield, and M. C. Malin (2001), Global mapping of Martian hematite mineral deposits: Remnants of water-driven processes on early Mars, *J. Geophys. Res.*, *106*(E10), 23,873–23,885, doi:10.1029/2000JE001415.

Clegg, S. M., E. Sklute, M. D. Dyar, J. E. Barefield, and R. C. Wiens (2009), Multivariate analysis of remote laser-induced breakdown spectroscopy spectra using partial least squares, principal component analysis, and related techniques, *Spectrochim. Acta B, 64*, 79–88.

Clement, B. G., G. W. Luther III, and B. M. Tebo (2009), Rapid, oxygen-dependent microbial Mn(II) oxidation kinetics at sub-micromolar oxygen concentrations in the Black Sea suboxic zone, *Geochim. Cosmochim. Acta*, *73*, 1878–1889.

Cloud, P. E., Jr. (1968), Atmospheric and hydrospheric evolution of the primitive Earth, *Science*, *160*, 729–736.

Cousin, A., O. Forni, S. Maurice, O. Gasnault, C. Fabre, V. Sautter, R. C. Wiens, and J. Mazoyer (2011), Laser induced breakdown spectroscopy library for the Martian environment, *Spectrochim. Acta, Part B, 66*, 805–814.

Crerar, D. A., R. K. Cormik, and H. L. Barnes (1980), Geochemistry of manganese: An overview, *Geology and Geochemistry of Manganese*, edited by I. M. Varentsov and G. Gasselly, vol. 1, pp. 293–334, E. Schweizerbart, Stuttgart, Germany.

Farley, K. A., et al. (2014), In situ radiometric and exposure age dating of the Martian surface, *Science*, *343*, 1247166-1-5, doi:10.1126/science.1247166.

Fischer, W. W., and A. H. Knoll (2009), An iron shuttle for deepwater silica in Late Archean and early Paleoproterozoic iron formation, *Geol. Soc. Am. Bull.*, *121*(1/2), 222–235.

Gellert, R., et al. (2006), Alpha Particle X-Ray Spectrometer (APXS): Results from Gusev crater and calibration report, *J. Geophys. Res.*, *111*, E02S05, doi:10.1029/2005JE002555.

Goetz, W., et al. (2005), Indication of drier periods on Mars from the chemistry and mineralogy of atmospheric dust, *Nature*, *436*, 62–65.

Grotzinger, J. P., et al. (2014), A habitable fluvio-lacustrine environment at Yellowknife Bay, Gale crater, Mars, *Science*, *343*, 1242777-1-14, doi:10.1126/science.1242777.

Halevy, I. (2013), Production, preservation, and biological processing of mass-independent sulfur isotope fractionation in the Archean surface environment, *Proc. Natl. Acad. Sci. U.S.A.*, *110*(44), 17,631–17,637.

Hansel, C. M., C. A. Zeiner, C. M. Santelli, and S. M. Webb (2012), Mn(II) oxidation by an ascomycete fungus is linked to superoxide production during asexual reproduction, *Proc. Natl. Acad. Sci. U.S.A.*, *109*(31), 12,621–12,625.

Haskin, L. A., et al. (2005), Water alteration of rocks and soils on Mars at the Spirit rover site in Gusev crater, *Nature*, *436*, 66–69.

Hazen, R. M., D. Papineau, W. Bleeker, R. T. Downs, J. M. Ferry, T. J. McCoy, D. A. Sverjensky, and H. Yang (2008), Mineral evolution, *Am. Mineral.*, *93*, 1693–1720.

Hecht, M. H., et al. (2009), Detection of perchlorate and the soluble chemistry of Martian soil at the Phoenix Lander site, *Science*, *325*, 64–67.

Herkenhoff, K. E., et al. (2004), Textures of the soils and rocks at Gusev crater from Spirit's microscopic imager, *Science*, *305*, 824–826.

Holland, H. D. (1984), *The Chemical Evolution of the Atmosphere and Oceans*, 582 pp., Princeton Univ. Press, Princeton, N. J.

Horsburgh, M. J., S. J. Wharton, M. Karavolos, and S. J. Foster (2002), Manganese: Elemental defence for a life without oxygen?, *Trends Microbiol.*, *10*(11), 496–501.

Hunten, D. M. (1979), Possible oxidant sources in the atmosphere and surface of Mars, *J. Mol. Evol.*, *14*, 71–78.

Hurowitz, J. A., W. W. Fischer, N. J. Tosca, and R. E. Milliken (2010), Origin of acidic surface waters and the evolution of atmospheric chemistry on early Mars, *Nat. Geosci.*, *3*, 323–326.

Johnson, J. E., S. M. Webb, K. Thomas, S. Ono, J. L. Kirchvink, and W. W. Fischer (2013), Manganese-oxidizing photosynthesis before the rise of cyanobacteria, *Proc. Natl. Acad. Sci. U.S.A.*, *110*(28), 11,238–11,243.

Lanza, N. L., S. M. Clegg, R. E. McInroy, R. C. Wiens, H. E. Newsom, and M. D. Deans (2012), Examining natural rock varnish and weathering rinds with laser-induced breakdown spectroscopy for application to ChemCam on Mars, *Appl. Opt.*, *51*(7), B74–B82.

Lanza, N. L., et al. (2013), Searching for rock surface alteration on Mars with the ChemCam laser-induced breakdown spectroscopy instrument. SCIX 2013, Milwaukee, Wisc., 29 Sept.-4 Oct. 2013.

Lanza, N. L., et al. (2014a), Manganese trends with depth on rock surfaces in Gale crater, Mars 45th Lunar and Planetary Science Conference, 17–21 Mar., Houston, Tex., no. 2599.

Lanza, N. L., et al. (2014b), Understanding the signature of rock coatings in laser-induced breakdown spectroscopy data, *Icarus*, doi:10.1016/j.icarus.2014.05.038, in press.

Learman, D. R., B. M. Voelker, A. S. Madden, and C. M. Hansel (2013), Constraints on superoxide mediated formation of manganese oxides, *Front. Microbiol.*, *262*, 1–11, doi:10.3389/fmicb.2013.00262.

Leshin, L. A., et al. (2013), Volatile, isotope, and organic analysis of Martian fines with the Mars Curiosity rover, *Science*, *341*, 1238937-1-9, doi:10.1126/science.1238937.

Luther, G. W. (2010), The role of one- and two-electron transfer reactions in forming thermodynamically unstable intermediates as barriers in multi-electron redox reactions, *Aquat. Geochem.*, *16*, 395–420.

Mahaffy, P. R., et al. (2013), Abundance and isotopic composition of gases in the Martian atmosphere from the Curiosity rover, *Science*, *341*, 263–266.

Maurice, S., et al. (2012), The ChemCam instrument suite on the Mars Science Laboratory (MSL) rover: Science objectives and mast unit description, *Space Sci. Rev.*, *170*, 95–166.

Maynard, J. B. (2010), The chemistry of manganese ores through time: A signal of increasing diversity of Earth-surface environments, *Econ. Geol.*, *105*, 535–552.

McLennan, S. M., et al. (2005), Provenance and diagenesis of the evaporate-bearing Burns formation, Meridiani Planum, Mars, *Earth Planet. Sci. Lett.*, *240*, 95–121.

McLennan, S. M., et al. (2014), Elemental geochemistry of sedimentary rocks in Yellowknife Bay, Gale Crater, Mars, *Science*, *343*, 1244734-1-10, doi:10.1126/science.1244734.

McSween, H. Y., et al. (2004), Basaltic rocks analyzed by the Spirit rover in Gusev crater, *Science*, *305*, 842–845.

Meslin, P.-Y., et al. (2013), Soil diversity and hydration as observed by ChemCam at Gale crater, Mars, *Science*, *341*, 1238670-1-10, doi:10.1126/science.1238670.

Morgan, J. J. (2005), Kinetics of reaction between O_2 and Mn(II) species in aqueous solutions, *Geochim. Cosmochim. Acta*, *69*(1), 35–48.

Morris, R. V., et al. (2004), Mineralogy at Gusev crater from the Mössbauer spectrometer on the Spirit rover, *Science*, *305*, 833–836.

Morris, R. V., et al. (2006), Mössbauer mineralogy of rock, soil, and dust at Gusev crater, Mars: Spirit's journey through weakly altered olivine basalt on the plains and pervasively altered basalt in the Columbia Hills, *J. Geophys. Res.*, *111*, E02S13, doi:10.1029/2005JE002584.
Myers, C. R., and K. H. Nealson (1988), Bacterial manganese reduction and growth with manganese oxide as the sole electron acceptor, *Science*, *240*, 1319–1321.
Nachon, M., et al. (2014), Calcium sulfate veins characterized by ChemCam/Curiosity at Gale crater, Mars, 2014. 45th Lunar and Planetary Science Conference, 17–21 Mar., Houston, Tex., no. 2006.
Ollila, A. M., et al. (2014), Trace element geochemistry (Li, Ba, Sr, and Rb) using Curiosity's ChemCam: Early results for Gale crater from Bradbury Landing Site to Rocknest, *J. Geophys. Res. Planets*, *119*, 255–285, doi:10.1002/2013JE004517.
Post, J. E. (1999), Manganese oxide minerals: Crystal structures and economic and environmental significance, *Proc. Natl. Acad. Sci. U.S.A.*, *96*(7), 3447–3454.
Raiswell, R., and D. E. Canfield (2012), The iron biogeochemical cycle past and present, *Geochem. Perspect.*, *1*(1), 1–220.
Sautter, V., et al. (2014), Igneous mineralogy at Bradbury Rise: The first ChemCam campaign at Gale crater, *J. Geophys. Res. Planets*, *119*, 30–46, doi:10.1002/2013JE004472.
Schmidt, M. E., et al. (2014), Geochemical diversity in first rocks examined by the Curiosity Rover in Gale Crater: Evidence for and significance of an alkali and volatile-rich igneous source, *J. Geophys. Res. Planets*, *119*, 64–81, doi:10.1002/2013JE004481.
Sellers, K., K. Weeks, W. R. Alsop, S. R. Clough, M. Hoyt, B. Pugh, and J. Robb (2007), *Perchlorate: Environmental Problems and Solutions*, 1st ed., 226 pp., CRC Press, Boca Raton, Fla.
Stumm, W., and J. J. Morgan (1996), *Aquatic Chemistry: Chemical Equilibria and Rates in Natural Waters*, 3rd ed., 1042 pp., John Wiley, New York.
Sunda, W. G., and D. J. Kieber (1994), Oxidation of humic substances by manganese oxides yields low-molecular-weight organic substances, *Nature*, *367*, 62–64.
Taylor, S. R., and S. M. McLennan (2009), *Planetary Crusts: Their Composition, Origin, and Evolution*, 378 pp., Cambridge Univ. Press, New York.
Tebo, B. M., H. A. Johnson, J. K. McCarthy, and A. S. Templeton (2005), Geomicrobiology of manganese(II) oxidation, *Trends Microbiol.*, *13*(9), 421–428.
Tosca, N. J., S. M. McLennan, B. C. Clark, J. P. Grotzinger, J. A. Hurowitz, A. H. Knoll, C. Schröder, and S. W. Squyres (2005), Geochemical modeling of evaporation processes on Mars: Insight from the sedimentary record at Meridiani Planum, *Earth Planet. Sci. Lett.*, *240*, 122–148.
Turekian, K. K., and K. H. Wedepohl (1961), Distribution of the elements in some major units of the Earth's crust, *Geol. Soc. Am. Bull.*, *72*(2), 175–192.
Wiens, R. C., et al. (2012), The ChemCam instrument suite on the Mars Science Laboratory (MSL) rover: Body unit and combined system performance, *Space Sci. Rev.*, *170*, 167–227.
Wiens, R. C., et al. (2013), Pre-flight calibration and initial data processing for the ChemCam laser-induced breakdown spectroscopy instrument on the Mars Science Laboratory rover, *Spectrochim. Acta B*, *82*, 1–27.
Yen, A. S., S. S. Kim, M. H. Hecht, M. S. Frant, and B. Murray (2000), Evidence that the reactivity of the Martian soil is due to superoxide ions, *Science*, *289*, 1909–1912.
Yen, A. S., et al. (2007), Nickel on Mars: Constraints on meteoritic material at the surface, *J. Geophys. Res.*, *111*, E12S11, doi:10.1029/2006JE002797.
Zahnle, K., R. M. Haberle, D. C. Catling, and J. F. Kasting (2008), Photochemical instability of the ancient Martian atmosphere, *J. Geophys. Res.*, *113*, E11004, doi:10.1029/2008JE003160.
Zent, A. P., and C. P. McKay (1994), The chemical reactivity of the Martian soil and implications for future missions, *Icarus*, *108*, 146–157.